Biophysical Journal, Volume *121*

Supplemental information

Pathological cardiolipin-promoted membrane hemifusion stiffens pulmonary surfactant membranes

Marilyn Porras-Gómez, Tooba Shoaib, Dylan Steer, Rosa Maria Espinosa-Marzal, and Cecília Leal

S1 TOPOGRAPHY AND SURFACE ROUGHNESS

Height-phase AFM maps with average surface roughness S_q of healthy (DPPC:DOPG 3:1, molar ratio) and diseased (+ CL 8 mol%) lipid-based PSM models in air at 85-90% RH and room temperature. Average surface roughness Sq was calculated from AFM topography images of area 5 x 5 μm with resolution of 521 x 521 data points (Table S1), using the discrete approximation of the root mean square (RMS), namely

$$S_q = \left[\frac{1}{L}\int_0^L Z(x)^2 dx\right]^{\frac{1}{2}} \approx \left[\frac{1}{N}\sum_{i=1}^{N} Z_i^2\right]^{\frac{1}{2}} \tag{S.1}$$

where L is the evaluation length, $Z(x)$ is the profile height function at x, N is the number of samples and Z_i is a sample of the profile height function.

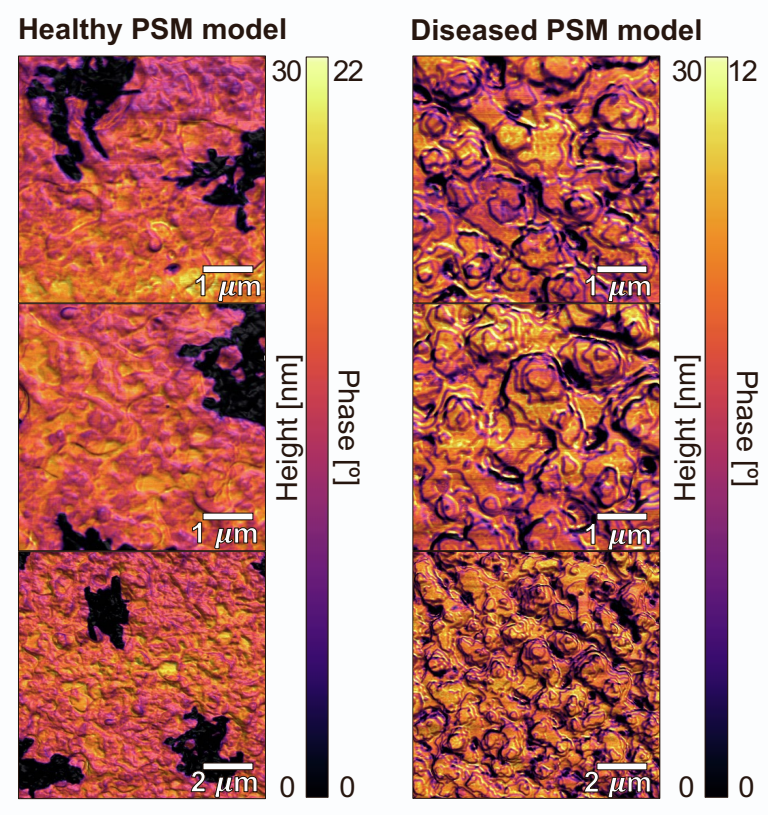

Figure S1: **AFM height-phase maps of the lipid-based PSM models**

Sample	Sq (nm)	SD (nm)	area (μm^2)	data points	n
Healthy PSM SLM	4.9	0.4	25	262144	2
Diseased PSM SLM	7.7	0.4	25	262144	2

Table S1: Average surface roughness

S2 STATISTICS OF FORCE MAP ANALYSIS

Force spectroscopy analysis at room temperature involved recording up to 5 different 5 μm x 5 μm or 1 μm x 1 μm force maps over 128 points x 128 lines (16384 data points) or 95 points and 256 lines (24576 data points). Measurements of Young's modulus E for the supported lipid multilayers (SLM) of bovine pulmonary surfactant membrane (PSM) extract in healthy (no cardiolipin (CL)) and diseased (with 8 mol% CL), and SLM of PSM model in healthy and diseased conditions were performed in air at 85-90% RH. While measurements of on supported lipid bilayers (SLB) of the model were performed in water.

Sample	Data Points	Adj. R2 (Gauss)	Mean E (MPa)	FWHM
Healthy bovine PSM	24576	0.966	32	9
Diseased bovine PSM	16384	0.994	90	30
Healthy PSM model	24576	0.995	41	8
Diseased PSM model	16384	0.974	51	29
Healthy SLB PSM model	16384	0.981	18	15
Diseased SLB PSM model	16384	0.957	30	22

Table S2: Statistics of force map analysis

S3 ANALYSIS OF ELASTICITY MEASUREMENTS

All reported Young's modulus E values result from the peak of a Gaussian fit of the elasticity distribution obtained from the respective force maps. The approximate value of E was calculated from the approaching curves by using the Hertz model for conical tips (Sneddon model) (1, 2):

$$E = \frac{\pi}{2}\frac{(1-\nu^2)}{tan(\theta)\delta^2}F \tag{S.2}$$

where F is the force of the tip that leads to an indentation depth δ in the sample with an angle θ, ν = 0.5 is the Poisson ratio of lipids (3).

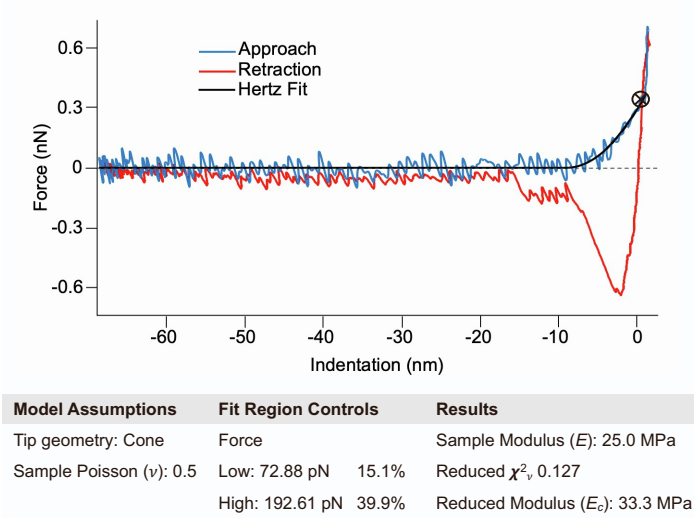

Model Assumptions	Fit Region Controls		Results
Tip geometry: Cone	Force		Sample Modulus (E): 25.0 MPa
Sample Poisson (ν): 0.5	Low: 72.88 pN	15.1%	Reduced χ^2_ν 0.127
	High: 192.61 pN	39.9%	Reduced Modulus (E_c): 33.3 MPa

Figure S2: **Hertzian fitting. Example of experimental force-indentation curve of the lipid healthy PSM model and the data fitting parameters. Typically, the fitting was of 40% of force**

.

S4 THICKNESS OF SUPPORTED LIPID BILAYERS

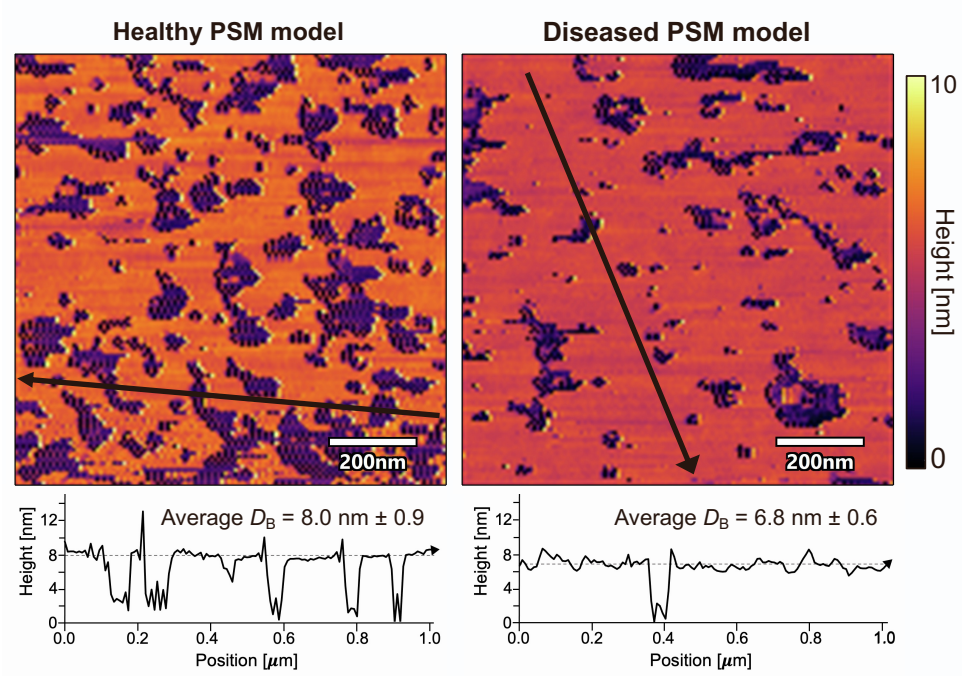

Figure S3: **Bilayer thickness. The thickness of supported lipid bilayers (SLB) was determined by AFM-in fluid topography. Purple areas correspond to uncovered SiO_2 substrates and yellow-orange areas correspond to one supported lipid bilayer. We report average bilayer thickness D_B with standard deviation for healthy and diseased PSM lipid models. We calculated D_B by measuring 8 cross-section lines of 3 different AFM images giving $n = 24$ per sample (healthy and diseased).**

S5 VALUES OF STRETCH K_A AND BENDING MODULUS κ_C

Sample	K_A (pN/nm)	κ_C (k_BT)
Healthy bovine PSM	341	160
Diseased bovine PSM	960	450
Healthy PSM model	437	205
Diseased PSM model	544	255
Healthy SLB PSM model	192	90
Diseased SLB PSM model	320	150

Table S3: Calculated K_A and κ_C

S6 EFFECT OF CHOLESTEROL ON THE PSM MODEL

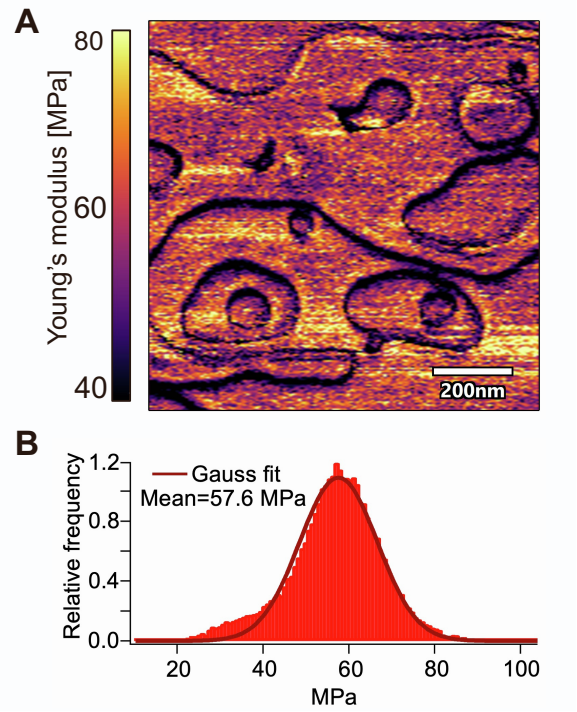

Figure S4: **Healthy SLM of PSM model with cholesterol. Preliminary data of Young's modulus map of healthy system containing 15 mol% cholesterol (A) and its corresponding Young's modulus distribution (B).**

S7 MODEL FOR INTERMEMBRANE FORCES

$$W = W_{\mathrm{DLVO}} + W_{\mathrm{ster}} + W_{\mathrm{hyd}} + W_{\mathrm{agg}} \tag{S.3}$$

The model (Eq. S.3) accounts for the most important inter- and intramolecular interactions in lipid bilayers used to calculate the energy potential E, which is related to the interaction energy per unit area through $W = E/a$; a is the lipid area. In SFA experiments, we measure F, the interbilayer force, which is related to the interaction energy W by the Derjaguin approximation: $W = F/2\pi R$, R being the radius of curvature of the mica surfaces (R =2 cm). Intermembrane forces include van der Waals (vdW), electrical double-layer, short range (repulsive) hydration and (attractive) hydrophobic forces (4, 5). DLVO theory accounts well for electrical double-layer (EDL) forces and vdW attractive forces but cannot predict bilayer fusion. At interbilayer distances ($d \lesssim$ 1-3 nm), a strong repulsion consisting of steric (hydration) forces and undulation forces dominates over the DLVO force. The steric hydration force exponentially decays with d ($E_{\mathrm{ster}} = C_{\mathrm{ster}} exp(-d/D_{\mathrm{ster}})$), with a decay length D_{ster} of the order of the hydration shell of the hydrophilic headgroups (typical range 0.2–1 nm) (6). Alternatively, steric hydration forces have been modeled by Alexander-de Gennes theory (7), i.e., assuming the headgroups' thermal fluctuations in a good solvent behave like a polymer brush. Due to their short-ranged nature, steric hydration forces were originally considered to stem from water structuring (8). Further studies revealed its entropic origin (9), which arises from the overlap of protrusions and hydrated headgroups. Here, we used the first and most simple approach. Steric hydration forces are thus influenced by the extent of lipid protrusion and the size of the hydrated headgroups, and hence, by their hydration strength. We assumed $D_{\mathrm{ster}} = 0.9nm$, as in previous (6), while C_{ster} is a fitting parameter. On the other hand, longer-range undulation forces W_{und} arise from the confinement of the bilayer ripples (undulations). Hence, the bending modulus of the lipid bilayers, which is mostly affected by the phase of the lipids, is a key property affecting W_{und}. The phase of the lipid domains depends on the length of the tail and its saturation, headgroup type, and temperature. However, W_{und} is only significant when the lipid bilayers are "free-standing" and "unstressed." This can happen if bilayers are deposited on "polymer cushions" but a solid substrate like mica is known to suppress undulation forces. Finally, an empiric model has been proposed for the hydrophobic force between bilayers (6). For lipids in a liquid-like state, which can be easily deformed or depleted by applying stresses, the hydrophobic energy potential is given by $E_{\mathrm{hyd}} = -\gamma(a - a_0)exp(-d/D_{\mathrm{hyd}})$, where $a = a_0(1 - exp(-d/D_{\mathrm{hyd}}))^{-1/2}$, D_{hyd} the decay length, γ the interfacial energy, and a and a_0 stressed and unstressed molecular areas, respectively. For bilayers in gel state, a is a weaker function of d due to their larger elastic modulus. The model also accounts for the self-aggregation energy between tails $E_{\mathrm{agg}} = 2\gamma a_0 + \gamma/a(a - a_0)^2$ (6), which includes the elastic deformation of the bilayer, headgroup repulsions and the surface tension. To directly compare the experiments $W_{\mathrm{exp}} = F/(2\pi R)$ with the model, the energy is referenced to the energy at $d = \infty$, i.e., $W(d) - W(\infty)$.

The model was first fit only at large separations ($D >$ 20 nm), where only the electrical double layer force is relevant, and other contributions in Eq. S.3 can be neglected. Hence, the long–range surface force is fit by the DLVO model, which gives the DLVO force as the sum of van der Waals F_{VDW} and electric double layer forces F_{EDL}:

$$\frac{F_{\mathrm{DLVO}}}{R} = \frac{F_{\mathrm{VDW}}}{R} + \frac{F_{\mathrm{EDL}}}{R} = -\frac{A_{\mathrm{H}}}{6D^2} + 4\pi\varepsilon\varepsilon_0\kappa\phi_0^2 exp(-\kappa D) \tag{S.4}$$

A_{H} being the Hamaker constant ($1.966x10^{-20}J$), D the separation between mica surfaces, $R_{\mathrm{eff}} = R$ the radius of the surface ($R = 2cm$), κ the inverse of the Debye length $\kappa = 1/\lambda_{\mathrm{EDL}}$, ϕ_0 the surface potential, ε the relative permittivity of the solution (unitless) and ε_0 the vacuum permittivity. The expression for the EDL force assumes constant surface potential. It is important to emphasize, that the expression for the EDL force was derived from a linearization of the Poisson-Boltzman equation that is only strictly valid for small potentials (<25 mV). The errors introduced by this linearized approach are typically not excessive for potentials as high as 200 mV, except for distances that are significantly shorter than one Debye length. The fitting parameters are the Debye length and the surface potential, which are determined to be $\lambda_{\mathrm{EDL}} \approx 28.7 \pm 3.0nm$ and $\phi_0 \approx 106 \pm 25mV$ in good approximation. The Debye length corresponds to an ionic strength in a 1:2 electrolyte of 0.038 ± 7 mM, while the ionic strength of the 0.15 mM lipid solution with 8 mol% cardiolipin is 0.036 mM.

To determine the percentage of charged cardiolipin in the membrane that is responsible for the surface potential determined from surface force measurements, the following expression was used:

$$\approx \frac{\sigma e_{\mathrm{c}} a_0}{X_z} \tag{S.5}$$

σ being the surface charge of the diseased membrane, $z = 2$ the number of charges per CL molecule, the electron charge $e_c = 1.6x10^{-19}C$, and X gives the percentage of CL in the membrane, which is assumed to be 8 mol%, as the CL in the lipid solution. The parameter a_0 is taken as the unstressed average area per lipid molecule in the bilayer. We assume a value of $a_0 \approx 67\text{Å}^2$, which is in the range of the reported values for DPPC with 7 mol% CL (10). This value considers that the presence of CL in the membrane increases the area per lipid molecule. The Grahame equation was used to roughly estimate the charge σ of an isolated membrane surface (11). Note that in our experiment, we measure the intermembrane interaction when we approach the surfaces against each other, and hence, the model does not strictly apply to the conditions of the experiment, but it enables us to estimate the order of magnitude of the surface charge. For a 1:2 electrolyte,

$$\sigma^2 = 2\varepsilon\varepsilon_0 kTC_\infty(exp(2e\phi_0/kT) + 2exp(-e\phi_0/kT) - 3)^2 \tag{S.6}$$

This yields $\sigma \approx -63.6 \pm 3.5C/cm^2$ and $17 \pm 1\%$ is the estimated number of dissociated CL molecules in the membrane. In a few experiments we calculated a much larger surface charge corresponding to $85 \pm 10\%$ dissociated CL molecules in the bilayer.

To determine the interfacial energy, Eq. S.3 was fit to the experimental results, using the known parameters for the DLVO contribution. For the decay lengths of the steric and hydrophobic terms, we have taken $D_{\text{hyd}} = 1.2nm$ and $D_{\text{ster}} = 0.9nm$, within the typical range for these decay lengths (6). The parameters of interfacial tension γ and C_{ster} were used as the fitting parameters. This yields $C_{\text{ster}} = 0.41 \pm 0.14x10^{-20}J$ and γ between 23 and 41 mJ/m^2. Typical values for γ range from 20–50 mJ/m^2 (6).

S8 LONG-RANGE FORCES

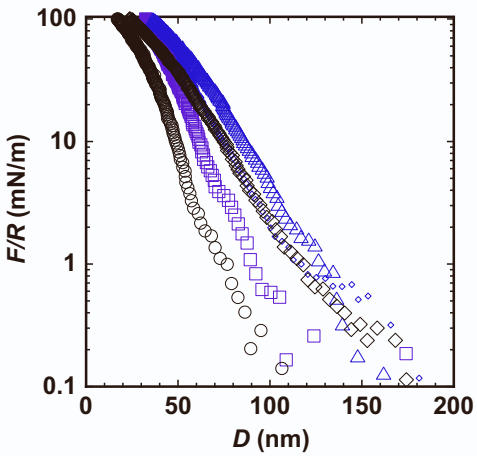

Figure S5: **Long-range force F vs. D for healthy inter-vesicle forces. A compression up to 100 mN/m does not lead to vesicle fusion in the absence of CL, indicating that the membrane fusion energy is much higher.**

S9 CARDIOLIPIN PROMOTES A STRUCTURAL CHANGE OF THE LIPID MICRODOMAINS UPON COMPRESSION

A film-thickness transition (Δ_w) with a change in thickness of $\approx 0.6 \pm 0.1$ nm was measured and the transition was reversible upon unloading. Such structural changes could reflect a rearrangement of lipid domains upon an applied stress, as recently demonstrated for other systems (12). In two additional experiments (e.g. green curve in Fig. S6), this structural transition did not happen upon the same range of compressions, perhaps suggesting that the composition of the compressed bilayers was different upon reformation.

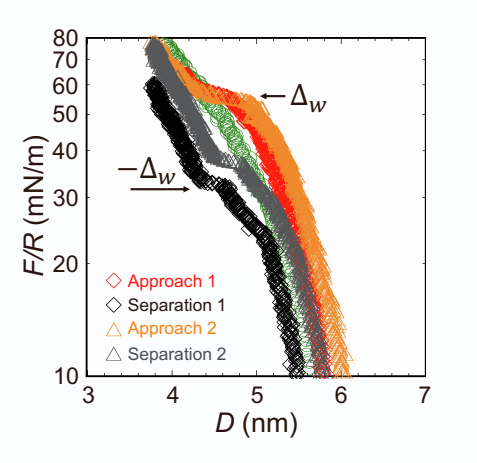

Figure S6: **Reversible structural transition upon compression of the bilayer approach (loading, orange, red, green) and separation (unloading, black and grey). The green circles could correspond to a different bilayer composition.**

S10 SUPPORTING REFERENCES

1. Krieg, M., G. Fläschner, D. Alsteens, B. M. Gaub, W. H. Roos, G. J. Wuite, H. E. Gaub, C. Gerber, Y. F. Dufrêne, and D. J. Müller, 2019. Atomic force microscopy-based mechanobiology. *Nat Rev Phys* 1:41–57.

2. Sicard, D., L. E. Fredenburgh, and D. J. Tschumperlin, 2017. Measured pulmonary arterial tissue stiffness is highly sensitive to AFM indenter dimensions. *J Mech Behav Biomed Mater.* 74:118–127.

3. Terzi, M. M., M. Deserno, and J. F. Nagle, 2019. Mechanical properties of lipid bilayers: A note on the Poisson ratio. *Soft matter* 15:9085–9092.

4. Helm, C., J. Israelachvili, and P. McGuiggan, 1989. Molecular mechanisms and forces involved in the adhesion and fusion of amphiphilic bilayers. *Science* 246:919–922.

5. Helm, C. A., J. N. Israelachvili, and P. M. McGuiggan, 1992. Role of hydrophobic forces in bilayer adhesion and fusion. *Biochemistry* 31:1794–1805.

6. Donaldson, S. H., C. T. Lee, B. F. Chmelka, and J. N. Israelachvili, 2011. General hydrophobic interaction potential for surfactant/lipid bilayers from direct force measurements between light-modulated bilayers. *PNAS* 108:15699–15704.

7. Schrader, A. M., S. H. Donaldson, J. Song, C.-Y. Cheng, D. W. Lee, S. Han, and J. N. Israelachvili, 2015. Correlating steric hydration forces with water dynamics through surface force and diffusion NMR measurements in a lipid–DMSO–H2O system. *PNAS* 112:10708–10713.

8. Israelachvili, J. N., and R. M. Pashley, 1983. Molecular layering of water at surfaces and origin of repulsive hydration forces. *Nature* 306:249–250.

9. Israelachvili, J., and H. Wennerström, 1996. Role of hydration and water structure in biological and colloidal interactions. *Nature* 379:219–225.

10. Wilson, B. A., A. Ramanathan, and C. F. Lopez, 2019. Cardiolipin-dependent properties of model mitochondrial membranes from molecular simulations. *Biophys. J.* 117:429–444.

11. Israelachvili, J., 2011. Intermolecular and Surface Forces. Academic Press, Burlington, MA, USA, third edition.

12. Lee, D. W., K. Kristiansen, S. H. D. Jr., N. Cadirov, X. Banquy, and J. N. Israelachvili, 2015. Real-time intermembrane force measurements and imaging of lipid domain morphology during hemifusion. *Nat. Commun.* 6:1–8.